

Tailoring the efficiency of 3D wire-shaped photovoltaic cells (WPVCs) by functionalization of solid–liquid interfacial properties

Jin Yan¹, M. Jasim Uddin¹, Tarik J. Dickens^{1,2}, Deborah E. Daramola¹, David Olawale^{1,2}, and Okenwa I. Okoli^{*1}

¹High Performance Materials Institute, Florida State University, 2005 Levy Ave., Tallahassee, FL 32303, USA

²NPGroup Inc., Tallahassee, FL 32311, USA

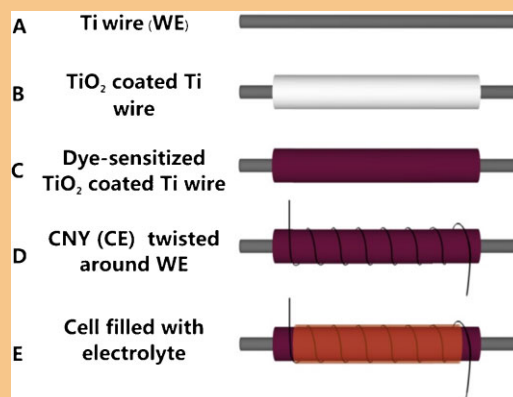
Received 23 August 2013, revised 26 September 2013, accepted 11 October 2013

Published online 27 November 2013

Keywords 3D PV cells, 3D photosensor, sol–gel method, wire-shaped cells

* Corresponding author: e-mail ookoli@fsu.edu, Phone: +1 850 645 8997, Fax: +1 850 410 6342

An efficient 3D dye-sensitized photovoltaic microwire has been developed using thermally stable and highly conductive titanium microwires and carbon nanotube yarns (CNYs). Interaligned, ultrastrong, and flexible CNYs with excellent mechanical integrity and electrocatalytic property were successfully used as counter electrodes (CEs). The TiO₂ nanophase coated Ti-microwire acts as the working electrode (WE). The CEs were twisted around the WE to collect and transmit the photogenerated electrons from the outer circuit. The interface in between photoactive TiO₂ film and 3D conductive support has been optimized. The optimized 3D WPVC shows a 0.583% photon to energy conversion efficiency under an irradiation of AM 1.5 (100 mW cm⁻²). Cells with various lengths were observed to attain a fill factor (*FF*) above 0.8. This work tested WPVCs under different working environments to assess their engineering potential.



© 2013 WILEY-VCH Verlag GmbH & Co. KGaA, Weinheim

1 Introduction The world energy demand and increasing global concern over climate change has focused research attention on renewable and clean energy sources. Photovoltaics (PVs) are promising examples, which have displayed rapid growth in recent times [1]. However, higher energy costs, when compared to traditional power generation methods, have thus far prevented PV from supplying a significant portion of the world's stationary energy [2]. In recent years, high efficiency dye-sensitized PV cells have been fabricated in many ways, with the most impressive cells reaching photon to energy conversion efficiencies of up to ~12% using platinized FTO (fluorine doped tin oxide) [3–6]. However, these PV cells have many restrictions due to

their rigid structures and high sheet resistance [7]. Several recent research reports on flexible DSSC are distinctively carried out on polymer supported transparent conductive oxide electrodes [8–11]. Ito et al. [12] and Yamaguchi et al. [11] reported that the photoenergy conversion efficiency ($\eta_{AM\ 1.5}$) with flexible 2D DSSC using titanium or plastic supported indium-doped tin oxide (ITO) flexible sheet reached up to 7.6%. However, photovoltaic wires have opened up an innovative feasibility for cost-effective and scalable solar energy harvesting system with potential textile applications [13]. A few recent reports discussed the fabrication of WPVCs using metal wires as working electrodes (WE) in combination with solid electrolytes that

show energy conversion efficiencies of up to 0.2% [14]. Some reports indicate that the efficiency could be increased if the DSSCs are assembled with liquid electrolyte and glass cladding [15–17], which yields limited sustainability during transportation and installation. The rapid developing optoelectronic industry, especially for the portable and highly integrated micro-electronic equipment, shows space limitations and necessitates cell flexibility and capability for changing shapes [18, 19]. Moreover, overcoming operating restrictions in the synthesis of these highly efficient flexible photovoltaic wires, with 3D features exhibiting long-term stability and reproducibility, remains a great challenge [7]. The progress in the wire-shaped solar cells has been summarized recently [20], especially; the carbon nanotubes (CNTs) have outstanding functions on enriching the WPVCs [7]. Even though the cells using Pt wire as CEs have already reached up to 5–7%, carbon materials can still maintain good flexibility and long life time when meeting the

practical engineering application [7, 16, 21]. The CE plays a key role in receiving electrons from the outer circuit and reducing the electrolyte redox mediator (I^-/I_3^-) [22–25]. However, CNTs are proved to have a catalytic effect on the couple of I^-/I_3^- . Therefore, it is worth noting that, coated with Pt particles, CNTs become functional to enrich the reciprocity between Pt particles and electrolyte by decreasing resistance for electron transportation [7, 26–28]. The twisted cell structure not only ensures an efficient interface between CEs and sensitizers, but also supports the 3D sensing features. This paper reports on the (a) anchoring process of TiO_2 film around the Ti-microwire, (b) optimization of TiO_2 film thickness, (c) stability of the 3D cells with different thermal conditions, and (d) 3D feature with inter-cell connectivity and flexibility.

2 Materials and methods Ti-microwires (Alfa Aesar, $\Phi = 127 \mu\text{m}$) were ultrasonicated successively in



Jin Yan received the B.S. degree in Applied Physics from the Nankai University in China in 2011, and is expected to obtain her Ph.D. degree in Industrial & Manufacturing Engineering from Florida State University in May 2015. She has participated in a number of research programs at various institutions including: Nankai University; Institute of Physics & Beijing National Lab. for Condensed Matter Physics, Chinese Academy of Sciences. She is now working in High Performance Materials Institute, Florida State University, under the supervision of Dr. Okenwa Okoli. Her current research interests include design and fabrication of 3D photovoltaic sensors for *in situ* structure health monitoring (SHM) systems.



M. Jasim Uddin obtained his Ph.D. degree in Materials Science and Technology from the University of Turin, Italy. He is currently a visiting Assistant Professor in the Department of Industrial and Manufacturing Engineering at the FAMU-FSU College of Engineering and High-Performance Materials Institute, Florida State University, USA. Prior to joining in The Florida State University; he worked at Tulane University, LA and Shahjalal University of Science and Technology, Sylhet. He discovered *metal centered hybrid catalyst, self-cleaning* and *photochromic textiles* during his doctoral research. His research focus lies on the development of nanostructured hybrid materials for energy conversion, storage and integrated structural health

monitoring. In recognition of his outstanding discovery in hybrid functional materials, the Government of Peoples Republic of Bangladesh honored him with UGC Award in 2010. The extraordinary contributions that his doctoral research made to the advanced materials for engineering application have recently been adopted in a college text book (ISBN: 978-1-84755-870-1) published by the Royal Society of Chemistry Publishing, London.



Okenwa Okoli is Professor and Department Chair of Industrial and Manufacturing Engineering at the FAMU-FSU College of Engineering. He has worked extensively in the development of affordable and functional composite manufacturing technologies for which he has received several awards. With the increased utilization of composites in critical structures, Dr. Okoli's innovative research efforts include the development of integrated structural health sensing within advanced composites and concrete structures. He also focuses on the development of scalable technologies for the manufacture of customizable multiscale and multifunctional composite structures, integrated PV sensors and innovative 3D energy conversion systems. He has extensive experience in the transient nonlinear dynamic analysis of fiber reinforced composite structures. He has 7 US patent applications (awarded and pending) in the areas of advanced composites and multiscale composites manufacture, structural ceramics, and ubiquitous real-time structural health monitoring. He is a chartered engineer and a chartered scientist.

acetone, isopropanol, and ethanol for 10 min each. To synthesize a basal coating on the surface, these wires were sintered in 400 °C air for 15 min after dipping into 70 wt% nitric acid (Sigma–Aldrich) for 3 min. At this stage, the shiny metal color of Ti wires changed to yellow, indicating the formation of the TiO₂ thin film (basal coating). For simplification, the major TiO₂ coating process can be divided into three parts: pre-coating, main-coating, and post-coating. Pre-coating is the n-TiO₂ thin film, which was prepared following the method reported previously [29]. This subsurface thin film worked as a foundation layer for following the nanostructured and nanoporous TiO₂ layer. The oxidized Ti wires were then immersed into pre-formed TiO₂ colloids via dip-coating method [14], which leads to a nanostructured TiO₂ layer coated on the Ti substrates (WEs). The TiO₂-coated Ti wires were sintered at 350 °C for 5 min. This dip-coating-sintering process was repeated several times, where the number of repetitions determined the thickness of the TiO₂ thin film. After the main-coating, the Ti electrodes were sintered in 450 °C air for 60 min and then dipped into a post-coating solution (50 mM TiCl₄ in ethanol) for 12 h following a 450 °C heat treatment for 30 min. These treated electrodes were sensitized for 24 h by immersing into N719 (N719 = [tetrabutylammonium]2[Ru(4-carboxylic acid-40-carboxy-late-2,20-bipyridyl)2(NCS)2]) dye (0.05 M mixture of *tert*-butanol and acetonitrile (volume ratio = 1:1)). The sensitized electrodes were finalized by rinsing in ethanol and drying in air. For CEs, surface treatments of CNY ($\Phi = 75 \mu\text{m}$) can also be found in our previous work [14]. Figure 1A shows that CNYs were twisted around the pre-formed photo-anodes as mentioned previously. Both of which were then embedded into a capillary cladding (inner diameter is 0.8 mm and the outer diameter is 1.2 mm) (Fig. 1B). The capillary tube protects the cell from adverse environmental effects. The SEM images of dispersed CNY and nanostructured TiO₂ are also shown in Fig. 1C and D. The electrolyte (1.0 M 1-butyl-3-methylimidazolium iodide,

50 mM lithium iodide, 30 mM iodine, 0.5 M *tert*-butylpyridine, and 0.1 M guanidinium thiocyanate in the mixture of acetonitrile and valeronitrile (volume ratio = 85:15)) was then introduced into capillary via capillary suction. The WPVCs were sealed by transparent silicon rubber and the WPVCs were tested using a VersaSTAT3 (Electrochemical system with EIS capability, Princeton Applied Research, USA) at a potential scan rate of 50 mV/s cooperating with a solar simulator (Newport, Model 9129X, AM 1.5 illumination, light intensity 100 mW cm⁻²). The cell performance was characterized by several general standards: open-circuit voltage (V_{oc}), short-circuit current density (J_{sc}), fill factor (FF) and photon-to-current conversion efficiency (η). Consequently, the energy conversion efficiency was calculated by the equation of $\eta = J_{sc} \times V_{oc} \times FF/P_{in}$, where P_{in} corresponds to the input power (100 mW cm⁻²). A field emission scanning electron microscope (SEM) (JOEL JSM-7401F) was used to investigate the surface morphology and interface of electrodes.

3 Results and discussion Figure 2 shows the SEM images of Ti-microwires after different coating processes under various magnifications. The TiO₂ film should be mesoporous to enlarge the surface area for anchoring more sensitizers [30]. Note that the basal coating and nanoporous TiO₂ pre-coating can provide a base for the following mesoporous and photoactive TiO₂ microfilm. The lower firm thin layer increases the photocurrent by suppressing the charge recombination on the electrode [14]. This was also confirmed with a charge-recombination mathematical modeling study carried out by Ferber et al. [29]. After the main-coating ($\sim 5 \mu\text{m}$ for each layer) (Fig. 2G and H), the mesoporous TiO₂ structures show (Fig. 2I) significant

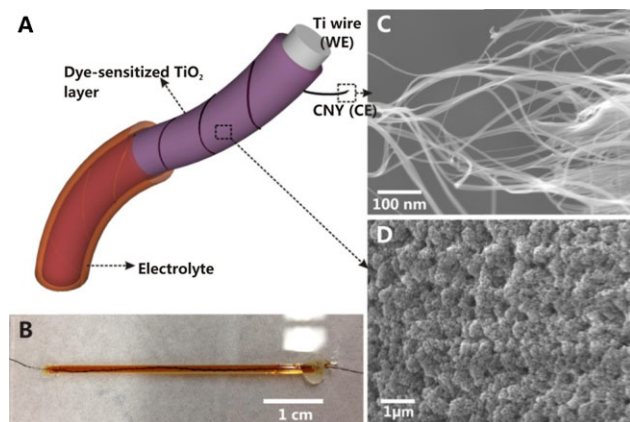


Figure 1 (A) Scheme of WPVC with liquid electrolyte. (B) Optical image of WPVC with glass cladding. (C) SEM image of the homogeneously distributed and interaligned carbon nanotubes in CNY (CE); (D) SEM image of porous TiO₂ surface.

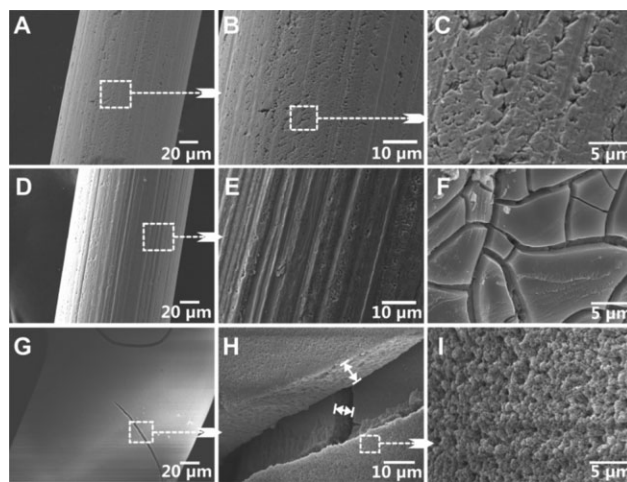


Figure 2 SEM images of (A) Ti-microwire after heat treatment (basal coating); (B and C) enlarged basal coating surface; (D) Ti-microwire after pre-coating; (E) enlarged pre-coating surface; (F) cracks on the pre-coating surface with a layer thickness about 1 μm ; (G) Ti-microwire after main-coating; (H) cracks on the main-coating surface with monolayer thickness about 5 μm ; (I) mesoporous TiO₂ surface with average particle size under 100 nm.

roughness throughout the film. This feature allows more dye molecules to be adsorbed into the active surface sites, which efficiently sensitizes the film in generating photoelectrons [31]. In addition, the mesoporous nature provides multidimensional channels for photogenerated electron transportation.

SEM images of CNYs (CE) before and after surface treatment are shown in Fig. 3A–D. The images are clearly indicative of the average diameter ($\phi = 20$ nm) of the individual carbon nanotubes (CNTs). The CNYs consist of numerous interaligned CNTs (Fig. 3D and 3D-inset), which is reported to exhibit high electrical conductivity, excellent electrocatalytic properties, outstanding mechanical properties [32], and significant structural flexibility [33–35]. These physiochemical characteristics of CNYs ensure operational flexibility and charge transportation feasibility of the WPVCs. From the comparison of high-resolution SEM images (Fig. 3B and D), it can be summarized that surface treatment of CNYs removes the sizing agent and functionalizes the exposed surface sites. Thus, the platinum nanoparticles are easily anchored to the external surface and make CNTs potentially electronegative in collecting photoelectrons from the outer circuits. In addition, the redox mediator (I^-/I_3^-) in the electrolyte deoxidizes the dye (N719) and the platinized CNY catalyzes the regeneration reaction of the mediator [36]. The large surface area is suitable for the reduction of triiodide (I_3^-), which actually improves the charge transportation and cell performance, correspondingly.

The PV performance of WPVCs was characterized using AM 1.5 solar simulator (100 mW cm^{-2}). The energy conversion efficiency (η) can be calculated by short-circuit current density (J_{sc}), open-circuit voltage (V_{oc}), fill factor (FF), and input power (P_{in}). The J – V curves of cells with different TiO_2 film thickness are shown in Fig. 4A. The WPVCs with different film thickness show an open-circuit

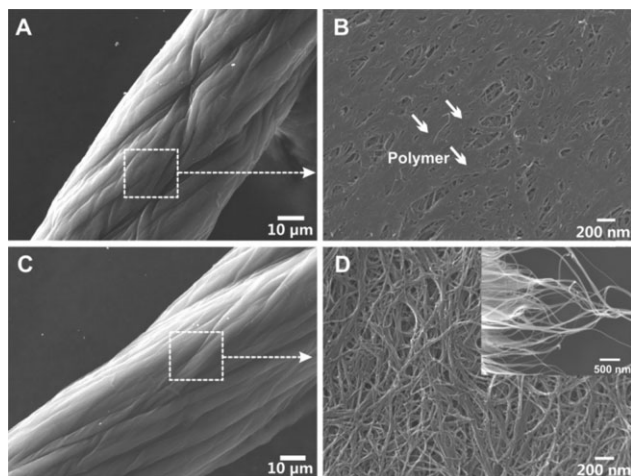


Figure 3 SEM images of (A) CNY without surface treatment; (B) enlarged view of the selected area in (A); (C) CNY after surface treatment; (D) enlarged view of the selected area in (C). The inset of (D) shows the general morphology of individual CNTs.

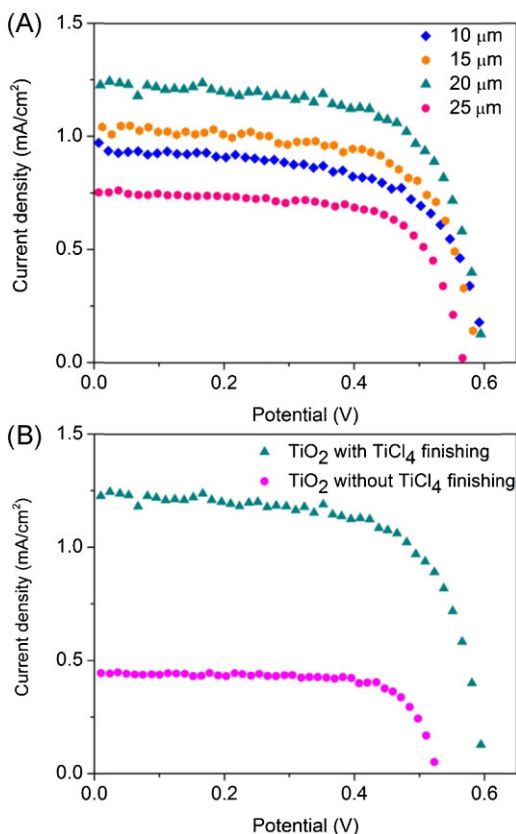


Figure 4 J – V curves of flexible WPVCs with (A) different TiO_2 layer thickness (2–5 layers ~ 10 – $25 \mu\text{m}$); and (B) different coating process.

voltage of approximately 0.60 V and maximum current density of 1.24 mA cm^{-2} . The WPVC with optimized TiO_2 film thickness ($20 \mu\text{m}$) shows the best cell performance ($FF = 0.67$) with efficient energy conversion efficiency ($\eta_{AM\ 1.5} = 0.4999\%$). The cell with higher film thickness shows an energy conversion efficiency below 0.3% .

The FF increased proportionally up to the TiO_2 film thickness of $20 \mu\text{m}$. Beyond this point, the PV performance of the WPVC reverses. The cells post-treated with TiCl_4 solution show comparatively better energy conversion efficiency than those that do not possess post-coating (Fig. 4B). With post-coating, J_{sc} has been improved from 0.44 to 1.24 mA cm^{-2} , which is a 282% increment. The post-treatment with TiCl_4 increases the roughness of the TiO_2 surface and extends the lifetime of photoelectrons [37, 38]. However, the relatively low efficiency is due to the rough interface between different TiO_2 nanophase and CEs. The integrity of supporting WEs, semiconducting phase, electrolyte, and CEs should be engineered for enhanced energy conversion efficiency and stability.

Carbon materials, such as CNT films, carbon fibers (CFs), etc., have been used as CEs in DSSCs for a long time [16]. However, the complicated structure of CNT thin film slows the charge transmission and retards the incoming light [39–41]. Self-aligned CNYs were used to replace the

conventional CEs. As mentioned above, the interaligned and entangled CNYs exhibit effective electrocatalytic activity with excellent electron transportation capability. In comparison with CFs, the CNYs show larger effective surface area. This feature potentially enhances the PV properties of the WPVCs [7, 16]. The interfacial properties of the CE was compared with control cells, which uses CNY at HPMI [42, 43] and silver wire as a CE. SEM characterization of our individual CNYs also indicates a porous and self-aligned network structure of the MWCNT yarn that is virtually free of catalyst particles or amorphous carbon particulates (Fig. 3D). Though the control WPVC with silver microwire exhibits the highest J_{sc} (2.29 mA cm^{-2}), it provides remarkably lower V_{oc} (70 mV), fill factor ($FF = 0.33$), and energy conversion efficiency of only 0.0525%. The WPVC with single CNY produces the highest energy conversion efficiency (0.499%). However, the cells with 3 CNYs and the HPMI CNYs show similar FF and energy conversion efficiencies ($\eta_{AM\ 1.5} = 0.40\%$) (Fig. 5A and B). As mentioned before, surface treatment functionalizes the CNTs and tailors the PV performance of the cells. The comparison of the energy conversion efficiency with other technical specifications is summarized in Fig. 5C. The WPVC with virgin CNY (CE) shows J_{sc} and V_{oc} of 0.37 mA cm^{-2} and 0.465 V , respectively. With this remarkable decrement in V_{oc} ($\Delta V_{oc} = 0.13 \text{ V}$) and J_{sc} ($\Delta J_{sc} = 0.868 \text{ mA cm}^{-2}$), this cell produced a photoconversion efficiency of 0.1222%. Furthermore, the conventional metal microwire shaped CEs (Pt, Ag wire, etc) are costly and easily corroded by liquid electrolytes [44–46]. However, the WPVC with virgin CNY (CEs) has adverse catalytic effects on the redox mediator (I^-/I_3^-), which allows light-generated electrons to react with I_3^- in the electrolyte [16, 47]. To avoid

these reverse catalytic effects and further improve the cell performance, platinumized CNYs were introduced to the WPVC as a replacement of conventional CEs. CNYs with Pt nanoparticles become functional to enrich the reciprocity between electrolyte and Pt particles by decreasing resistance of charge-transfer [47]. The cells with platinumized CNYs enhance the J_{sc} from 0.57 to 1.24 mA cm^{-2} (a 218% improvement) (Fig. 5D), which was indicative of double photon to current conversion efficiency obtained without platinumized CEs.

The PV performance of the WPVCs with variable lengths (2.0–4.5 cm) are summarized in Fig. 6. In Fig. 6A, it is may be observed that short-circuit current (I_{sc}) is directly proportional to the cell length (from 0.0365 to 0.0448 mA), while J_{sc} decreases from 1.50 to 0.82 mA cm^{-2} with an increase in cell length. The results indicate that the increasing in I_{sc} cannot compete with increasing effective surface area. However, the FF and V_{oc} of these WPVCs remain stable. The variation in V_{oc} ($\sim 0.47 \text{ V}$) with different cell lengths is negligible. Besides the 4.5 mm cell ($FF = 0.78$), all the other cells exhibit excellent FF s (> 0.80) (Fig. 6B). $J-V$ curves of WPVCs with different cell lengths are shown in Fig. 6C and the observable decrease in cell efficiency can be found in Fig. 6D. To further improve the efficiency stability at the applicable length, more self-aligned and interconnected CNTs could be taken into consideration to ensure fast electron transport capability [48].

Two WPVCs with similar $J-V$ performance were connected in parallel and series. The corresponding $I-V$ curves are included in Fig. 7A along with their individual $I-V$ curves. It is evident that the I_{sc} of two parallel cells ($70.99 \mu\text{A}$) is approximately the sum of their own I_{sc} , while the V_{oc} of two series cells (0.99 V) is equal to the sum of their

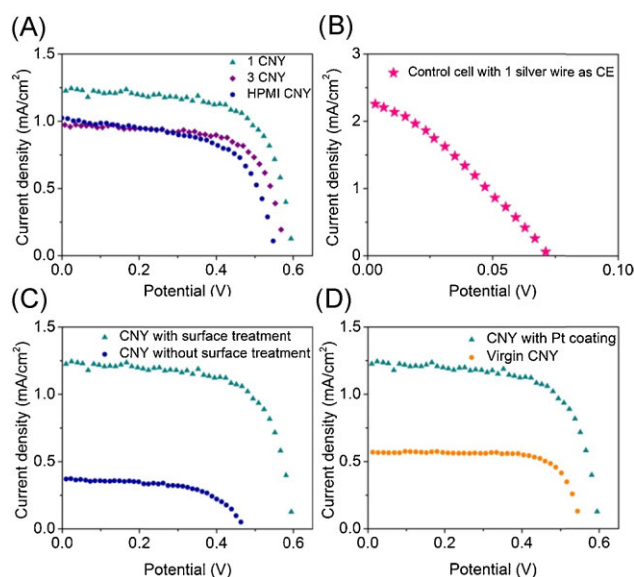


Figure 5 $J-V$ curves of flexible WPVCs with (A and B) different CEs (1CNY, 3CNY, HPMI CNY, 1 silver wire); (C) different CE surface treatment methods (if apply surface treatment for CNYs); (D) different treatment for CEs (if apply Pt coating on CNYs).

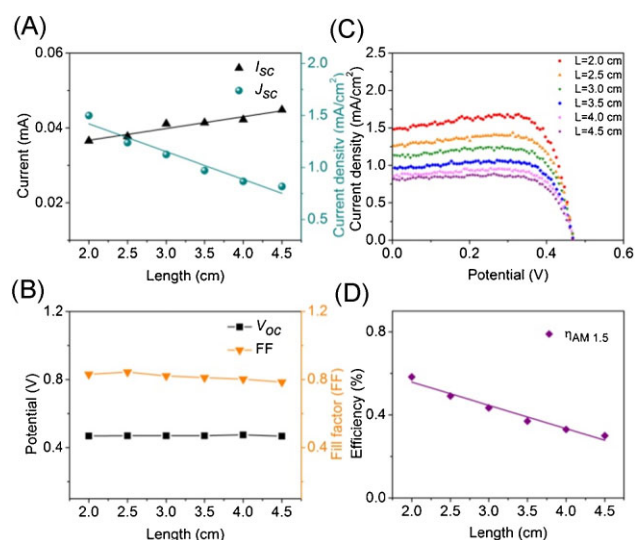


Figure 6 (A) Relative short-circuit current and current density of WPVCs with different cell lengths; (B) relative open-circuit voltage and fill factor of PV cells with different cell lengths; (C) $J-V$ curves of PV cells using 1 CNY as CE with different cell lengths; (D) change in PV cells' performance with different cell lengths.

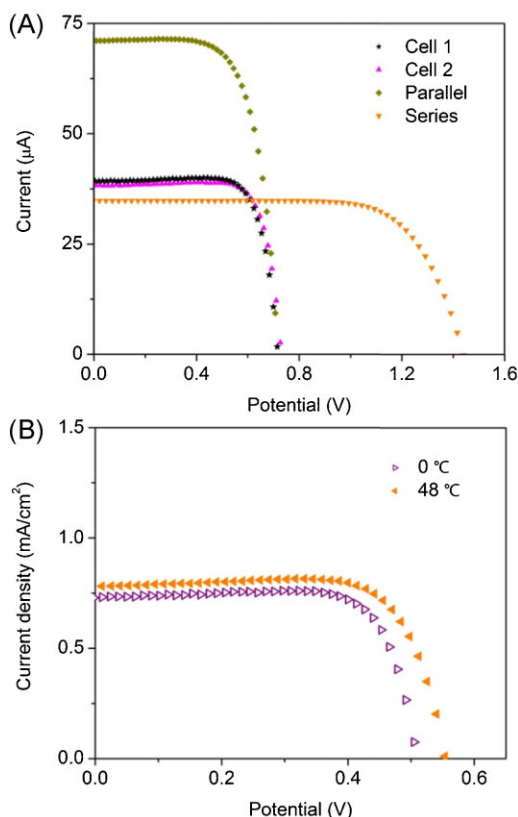


Figure 7 (A) I - V curves of two similar WPVCs under different connections (parallel and serious); (B) J - V curves of WPVC under different working temperatures (0 and 48 °C).

open-circuit voltages. The connection between two cells causes an inevitable resistance for the whole circuit, which is the reason why the sum I_{sc} cannot be exactly doubled [14, 25, 49, 50]. These results confirm that different connections may improve the cell performance in various ways, which can potentially be useful for required engineering applications. According to the Arrhenius's law, J_{sc} exhibits exponential growth with increasing temperature [52]. In addition, a corresponding decrease in cell resistance can result in an improvement in FF [51]. In Fig. 7B, the cell performance under different working temperatures (0 and 48 °C) is compared. The J_{sc} and V_{oc} were slightly improved ($\Delta J_{sc} = 0.064 \text{ mA cm}^{-2}$ and $\Delta V_{oc} = 0.04 \text{ V}$) with increasing temperature. The FF is also enhanced with increasing temperature ($\Delta FF = 0.03$). This phenomenon infers that WPVCs are potentially enabled to maintain their PV performance stably under various working environments, which provides proof of success for applying WPVCs in practical SHM structures.

4 Conclusions Embeddable WPVCs with three-dimensional energy harvesting features were fabricated using Ti microwire as WEs and CNY as CEs. The photosensitive TiO_2 film thickness was optimized using a hydrothermal sol-gel method. It was found that WPVCs with film

thickness of approximately 20 μm show the best photon-to-current energy efficiency. The functional surface and interface of the CE play an important role in energy conversion process. The WPVC with 1 Pt/CNY produces a 0.4999% energy conversion efficiency under standard AM 1.5 light intensity. By using the 3D energy harvesting capability, the WPVCs provide up to 0.5830% energy conversion efficiency. Furthermore, according to their stabilities under various working environments, WPVCs have capabilities for future engineering application.

Acknowledgements This work is supported by the U.S. National Science Foundation through grant ID CMMI-0969413. The authors also want to thank Dr. Mei Zhang (High-performance Materials Institute, Florida State University, FL, USA) for providing control CNYs.

References

- [1] M. Wright and A. Uddin, *Sol. Energy Mater. Sol. Cells* **107**, 87 (2012).
- [2] N. Espinosa, M. Hösel, D. Angmo, and F. C. Krebs, *Energy Environ. Sci.* **5**, 5117 (2012).
- [3] F. Gao, Y. Wang, D. Shi, J. Zhang, M. K. Wang, X. Y. Jing, R. Humphry-Baker, P. Wang, S. M. Zakeeruddin, and M. Grätzel, *J. Am. Chem. Soc.* **130**, 10720 (2008).
- [4] Q. J. Yu, Y. H. Wang, Z. H. Yi, N. N. Zu, J. Zhang, M. Zhang, and P. Wang, *ACS Nano* **4**, 6032 (2010).
- [5] F. Sauvage, D. H. Chen, P. Comte, F. Z. Huang, L. P. Heiniger, Y. B. Cheng, R. A. Caruso, and M. Grätzel, *ACS Nano* **4**, 4420 (2010).
- [6] M. K. Nazeeruddin, E. Baranoff, and M. Grätzel, *Sol. Energy* **85**, 1172 (2011).
- [7] J. Yan, M. J. Uddin, T. J. Dickens, and O. I. Okoli, *Sol. Energy* **96**, 239 (2013).
- [8] T. Miyasaka and Y. Kijitori, *J. Electrochem. Soc.* **151**, A1767 (2004).
- [9] S. Uchida, M. Tomiha, H. Takizawa, and M. Kawaraya, *J. Photochem. Photobiol. A* **164**, 93 (2004).
- [10] M. Durr, A. Schmid, M. Obermaier, S. Rosselli, A. Yasuda, and G. Nelles, *Nature Mater.* **4**, 607 (2005).
- [11] T. Yamaguchi, N. Tobe, D. Matsumoto, T. Nagai, and H. Arakawa, *Sol. Energy Mater. Sol. Cells* **94**, 812 (2010).
- [12] S. Ito, N. L. C. Ha, G. Rothenberger, P. Liska, P. Comte, S. M. Zakeeruddin, P. Pechy, M. K. Nazeeruddin, and M. Grätzel, *Chem. Commun.* 4004 (2006).
- [13] J. Ramier, C. J. G. Plummer, Y. Leterrier, J. A. E. Månson, B. Eckert, and R. Gaudiana, *Renew. Energ.* **33**, 314 (2008).
- [14] M. J. Uddin, T. Dickens, J. Yan, R. Chirayath, D. O. Olawale, and O. I. Okoli, *Sol. Energy Mater. Sol. Cells* **108**, 65 (2013).
- [15] A. Mishra, M. K. R. Fischer, and P. Bäuerle, *Angew. Chem. Int. Ed.* **48**, 2474 (2009).
- [16] S. Hou, X. Cai, Y. Fu, Z. Lv, D. Wang, H. Wu, C. Zhang, Z. Chu, and D. Zou, *J. Mater. Chem.* **21**, 13776 (2011).
- [17] Y. Fu, Z. Lv, H. Wu, S. Hou, X. Cai, D. Wang, and D. Zou, *Sol. Energy Mater. Sol. Cells* **102**, 212 (2012).
- [18] X. Fan, Z. Z. Chu, F. Z. Wang, C. Zhang, L. Chen, Y. W. Tang, and D. C. Zou, *Adv. Mater.* **20**, 592 (2008).
- [19] Q. Zeng, Y. Yu, L. Wu, B. Qi, and J. Zhi, *Phys. Status Solidi A* **207**, 2201 (2010).

- [20] T. Chen, L. Qiu, Z. Yang, and H. Peng, *Chem. Soc. Rev.* **42**, 5031 (2013).
- [21] Y. Fu, M. Peng, Z. Lv, X. Cai, S. Hou, H. Wu, X. Yu, H. Kafafy, and D. Zou, *Nano Energy*, **2**, 537 (2013).
- [22] N. Papageorgiou *Coord. Chem. Rev.* **248**, 1421 (2004).
- [23] T.N. Murakami and M. Grätzel, *Inorg. Chim. Acta* **361**, 572 (2008).
- [24] S. C. Hou, X. Cai, Y. P. Fu, Z. B. Lv, D. Wang, H. W. Wu, C. Zhang, Z. Z. Chu, and D. C. Zou, *J. Mater. Chem.* **21**, 13776 (2011).
- [25] M. J. Uddin, B. Davies, T. J. Dickens, and O. I. Okoli, *Sol. Energy Mater. Sol. Cells* **115**, 166 (2013).
- [26] T. Chen, L. Qiu, Z. Yang, Z. Cai, J. Ren, H. Li, H. Lin, X. Sun, and H. Peng, *Angew. Chem. Int. Ed.* **51**, 11977 (2012).
- [27] Z. Yang, H. Sun, T. Chen, L. Qiu, Y. Luo, and H. Peng, *Angew. Chem. Int. Ed.* **52**, 7545 (2013).
- [28] S. Pan, Z. Yang, H. Li, L. Qiu, H. Sun, and H. Peng, *J. Am. Chem. Soc.* **135**, 10622 (2013).
- [29] J. Ferber, R. Stangl, and J. Luther, *Sol. Energy Mater. Sol. Cells* **53**, 29–54 (1998).
- [30] M. Grätzel *J. Photochem. Photobiol. A* **164**, 3 (2004).
- [31] T. Dittrich *Phys. Status Solidi A* **182**, 447 (2000).
- [32] M. D. Lima, S. Fang, X. Lepró, C. Lewis, R. Ovalle-Robles, J. Carretero-González, E. Castillo-Martínez, M. E. Kozlov, J. Oh, N. Rawat, C. S. Haines, M. H. Haque, V. Aare, S. Stoughton, A. A. Zakhidov, and R. H. Baughman, *Science* **331**, 51 (2011).
- [33] O. Topon, D. Inaguma, K. Matsumoto, and N. T. Naoe, *ECS Trans.* **25**, 87 (2010).
- [34] E. Frackowiak and F. Beguin, *Carbon* **39**, 937 (2001).
- [35] T. Chen, L. B. Qiu, H. P. Li, and H. S. Peng, *J. Mater. Chem.* **22**, 23655 (2012).
- [36] J. H. Wu, Z. Lan, S. C. Hao, P. J. Li, J. M. Lin, M. L. Huang, L. Q. Fang, and Y. F. Huang, *Pure. Appl. Chem.* **80**, 2241 (2008).
- [37] B. C. O'Regan, J. R. Durrant, P. M. Sommeling, and N. J. Bakker, *J. Phys. Chem. C* **111**, 14001 (2007).
- [38] S. Ito, P. Liska, P. Comte, R. L. Charvet, P. Pechy, U. Bach, L. Schmidt-Mende, S. M. Zakeeruddin, A. Kay, M. K. Nazeeruddin, and M. Grätzel, *Chem. Commun.* 4351 (2005).
- [39] S. Barazzouk, S. Hotchandani, K. Vinodgopal, and P. V. Kamat, *J. Phys. Chem. B* **108**, 17015 (2004).
- [40] S. Zhang, C. Y. Ji, Z. Q. Bian, R. H. Liu, X. Y. Xia, D. Q. Yun, L. H. Zhang, C. H. Huang, and A. Y. Cao, *Nano. Lett.* **11**, 3383 (2011).
- [41] S. Huang, L. Li, Z. Yang, L. Zhang, H. Saiyin, T. Chen, and H. Peng, *Adv. Mater.* **23**, 4707 (2011).
- [42] M. Zhang, K. R. Atkinson, and R. H. Baughman, *Science* **306**, 1358 (2004).
- [43] D. Zhao, T. Liu, J. G. Park, M. Zhang, J.-M. Chen, and B. Wang, *Microelectron. Eng.* **96**, 71 (2012).
- [44] D. Zou, D. Wang, Z. Chu, Z. Lv, and X. Fan, *Coord. Chem. Rev.* **254**, 1169 (2010).
- [45] D. Y. Liu, M. Y. Zhao, Y. Li, Z. Q. Bian, L. H. Zhang, Y. Y. Shang, X. Y. Xia, S. Zhang, D. Q. Yun, Z. W. Liu, A. Y. Cao, and C. H. Huang, *ACS Nano* **6**, 11027 (2012).
- [46] L. Yuan, F. Chen, C. Zheng, J. Liu, and N. Alemu, *Phys. Status Solidi A* **209**, 1376 (2012).
- [47] S. Zhang, C. Y. Ji, Z. Q. Bian, P. R. Yu, L. H. Zhang, D. Y. Liu, E. Z. Shi, Y. Y. Shang, H. T. Peng, Q. Cheng, D. Wang, C. H. Huang, and A. Y. Cao, *ACS Nano* **6**, 7191 (2012).
- [48] A. Kongkanand and P. V. Kamat, *ACS Nano* **1**, 13 (2007).
- [49] J. Wan, G. Fang, P. Qin, Q. Zheng, N. Liu, N. Sun, Y. Tu, X. Fan, F. Cheng, and X. Zhao, *Sol. Energy Mater. Sol. Cells* **101**, 289 (2012).
- [50] J. Y. Tang, Z. Y. Huo, S. Brittan, H. W. Gao, and P. D. Yang, *Nature Nanotechnol.* **6**, 568 (2011).
- [51] M. Berginc, U. O. Krasovec, M. Jankovec, and M. Topic, *Sol. Energy Mater. Sol. Cells* **91**, 821 (2007).